Journal of Controlled Release 149 (2011) 225–235

Contents lists available at ScienceDirect

Journal of Controlled Release

journal homepage: www.elsevier.com/locate/jconrel

Transport of epidermal growth factor in the stroke-injured brain

Yuanfei Wang [a,b], Michael J. Cooke [a], Yakov Lapitsky [a,1], Ryan G. Wylie [c], Nadia Sachewsky [d], Dale Corbett [e], Cindi M. Morshead [b,d], Molly S. Shoichet [a,b,c,*]

[a] Department of Chemical Engineering and Applied Chemistry, University of Toronto, 200 College Street, Toronto, ON, Canada M5S 3E5
[b] Institute of Biomaterials and Biomedical Engineering, 164 College Street, Room 407, Toronto, ON, Canada M5S 3G9
[c] Department of Chemistry, University of Toronto, 80 St. George Street, Toronto, ON, Canada M5S 3H6
[d] Department of Surgery, University of Toronto, 160 College Street, Room 1006, Toronto, ON, Canada M5S 3E1
[e] BioMedical Sciences, Faculty of Medicine, Memorial University, St. John's, NL, Canada A1B 3V6

ARTICLE INFO

Article history:
Received 30 June 2010
Accepted 18 October 2010
Available online 27 October 2010

Keywords:
Stroke
Epidermal growth factor
Protein transport in brain
PEG modification
Integrative optical imaging
In vivo protein transport

ABSTRACT

Stroke is a neurological disorder that currently has no cure. Intrathecal delivery of growth factors, specifically recombinant human epidermal growth factor (rhEGF), stimulates endogenous neural precursor cells in the subventricular zone (SVZ) and promotes tissue regeneration in animal models of stroke. In this model, rhEGF is delivered with an invasive minipump/catheter system, which causes trauma to the brain. A less invasive strategy is to deliver rhEGF from the brain cortex; however, this requires the protein to diffuse through the brain, from the site of injection to the SVZ. Although this method of delivery has great potential, diffusion is limited by rapid removal from the extracellular space and hence for successful translation into the clinic strategies are needed to increase the diffusion distance. Using integrative optical imaging we investigate diffusion of rhEGF vs. poly(ethylene glycol)-modified rhEGF (PEG-rhEGF) in brain slices of both uninjured and stroke-injured animals. For the first time, we quantitatively show that PEG modification reduces the rate of growth factor elimination by over an order of magnitude. For rhEGF this corresponds to a two to threefold increase in predicted brain penetration distance, which we confirm with *in vivo* data.

1. Introduction

Each year more than 15 million stroke injuries occur worldwide, leading to 5 million deaths [1]. Stroke is a neurodegenerative condition caused by the occlusion or rupture of cerebral arteries [2,3]. Currently there is no cure for stroke, and the only FDA approved treatment is tissue plasminogen activator (tPA), a thrombolytic agent with limited therapeutic benefit [1].

An emerging trend in treating neurodegenerative disorders is the use of regenerative techniques [3–5]. One method for achieving regeneration is to stimulate endogenous stem cell proliferation and differentiation to promote repair. A population of neural stem cells and their progeny (together termed neural precursor cells, NPCs) are located in the subventricular zone (SVZ) of the lateral ventricles [6] and the dentate gyrus of the hippocampus [7]. Following stroke, there is an increase in proliferation of NPCs in the SVZ. In response to injury, the NPCs will migrate towards the site of injury [3]. However, the extent of regeneration after stroke is limited. It is proposed that administering exogenous factors could enhance this process and improve tissue regeneration and promote functional recovery.

A number of growth factors have shown functional benefits in animal models of stroke [8–11]; however, the methods of delivery are not ideal, thereby limiting clinical translation. Systemic delivery is inadequate because most drugs either cannot cross the blood-brain barrier (BBB) or lead to adverse systemic side effects at the high doses required [12]. Direct delivery to the tissue is not ideal because minipump/catheter systems are highly invasive when implanted in the brain and have the risk of infection. Therefore a minimally invasive delivery strategy, such as a drug delivery scaffold placed on the brain, is required (Supplementary Fig. 1S).

We first sought to define protein diffusion in the brain to understand whether protein released at a distant tissue site would reach the target cells. Protein transport in the brain is predominantly governed by: the intrinsic diffusivity (D) of the protein; tissue tortuosity ($\lambda = (D/D^*)^{1/2}$ where D^* is the protein's apparent diffusivity in brain); and removal from the diffusing protein population as denoted by the first order elimination rate constant k_e [13]. One challenge we face in developing a minimally invasive drug delivery system is that proteins are rapidly eliminated from the diffusion path *via* binding to the extracellular matrix (ECM) and cell-surface receptors [14]. Following binding, proteins are taken up by cells, enzymatically degraded or removed to the systemic circulation [14].

* Corresponding author. The Donnelly Centre, 160 College St., Room 514 Toronto, ON, Canada M5S 3E1. Tel.: +1 416 978 1460; fax: +1 416 978 4317.
E-mail address: molly.shoichet@utoronto.ca (M.S. Shoichet).
[1] Current Address: Department of Chemical and Environmental Engineering, University of Toledo, 2801 West Bancroft Street, Toledo, OH 43606, USA.

0168-3659/$ – see front matter © 2010 Elsevier B.V. All rights reserved.
doi:10.1016/j.jconrel.2010.10.022

This leads to only 1–2 mm penetration distances, which are often insufficient to reach the target site.

One strategy to improve protein penetration is to conjugate poly (ethylene glycol) (PEG) to the protein of interest to decrease its rate of elimination [15,16]. PEG is a hydrophilic polymer that acts as a stealth agent to mask proteins from cellular/macrophage uptake and enzymatic degradation [17–21]. While reports to date have provided some promising results, previous studies on the diffusion of proteins in tissues and the effect of PEG modification did not quantify the effect of PEG modification on elimination rate. Moreover, these previous studies used mixed populations of proteins with different degrees of modification [22,23], which complicates the analysis, making the effect of PEG modification difficult to assess.

Here we investigate the transport and elimination of recombinant human epidermal growth factor (rhEGF) and PEG-rhEGF in brain cortical tissue using *ex vivo* integrative optical imaging (IOI) [13]. This technique uses epi-fluorescent microscopy to determine transport properties of a diffusing protein population [13]. To the best of our knowledge, IOI has never been used to quantify protein elimination rate. Thus, our use of IOI to study drug elimination presents an important extension of this tool. Furthermore, IOI studies have not been previously conducted in brains with stroke injuries. However, given that neural injury, including stroke, affects the structural organization, cells and molecules in the brain tissue [4,24–27], it is important to study the transport of proteins in both injured and uninjured tissue. To gain further insight into tissue penetration, we compared the transport calculated in tissue slices to that in animals using a rhEGF ELISA.

Human EGF is a 6.2 kDa protein with three lysine amino acid residues, thus providing three amine groups as potential sites for PEG modification [28]. It is known that EGF induces proliferation of NPCs and stimulates generation of radial glial cells in the brain that support neuronal migration [29,30]. Kolb et al. showed that in an animal stroke model, infusion of rhEGF followed by erythropoietin into the lateral ventricle increased proliferation of NPCs and enhanced functional recovery [10].

We demonstrate that 5 kDa methoxy-PEG-propionaldehyde (mPEG-PPA) can be conjugated to rhEGF in a site-specific manner resulting in one of mono-(PEG_1), di (PEG_2), or tri-(PEG_3) PEG_x-rhEGF. Controlling the pH and reactant ratios results in higher yield than previously reported [31,32]. Using IOI, we demonstrate that mono-PEG modification reduces the rate of rhEGF elimination. Moreover, we show that stroke injuries lead to lower tissue tortuosity and higher rates of irreversible protein binding/elimination. The effect of PEG modification on rhEGF penetration distance is confirmed *in vivo* using a mouse stroke model. These data demonstrate the potential to increase penetration distance, thereby allowing for a minimally invasive delivery strategy where the protein does not need to be injected directly into the brain tissue but instead can be applied at the surface following stroke.

2. Materials and methods

2.1. Materials

Recombinant human epidermal growth factor (rhEGF) and the rhEGF ELISA detection kit were purchased from PeproTech Inc. (Rocky Hill, NJ, USA). Methoxy-poly(ethylene glycol, 5 kDa) activated with propionaldehyde (mPEG-PPA) or N-hydroxysuccinimide (mPEG-NHS) were purchased from NOF Corp. (Tokyo, Japan). Alexa Fluor 488-NHS, Alexa Fluor 488-hydrazide fluorescent dyes and 10× PBS buffered solution were obtained from Invitrogen Inc. (Burlington, ON, Canada). 4-(4,6-Dimethoxy-1,3,5-triazin-2-yl)-4-methylmorpholinium chloride (DMTMM), sodium cyanoborohydride ($NaCNBH_3$), NaCl, $MgCl_2$, $CaCl_2$, $BaCl_2$, Na_2HPO_3, NaH_2PO_3 TES, MES, ethylenediamine tetraacetic acid (EDTA), ethylene glycol-bis(2-aminoethyl)-N,N,N′, N′-tetraacetic acid (EGTA), phenylmethanesulfonyl fluoride (PMSF), dithioreitol, sodium acetate buffer salts, and low electroendosmosis (low EEO) agarose were supplied by Sigma Aldrich (Oakville, ON, Canada). Artificial cerebrospinal fluid (aCSF) and all buffers were prepared with distilled and deionized water prepared from a Millipore Milli-RO 10 Plus and Milli-Q UF Plus at 18 MΩ m resistivity (Millipore, Bedford, USA). MicroBCA protein assay kit was obtained from Thermo Fisher Scientific (Rockford IL, USA.) and used as per the manufactures instructions.

2.2. PEG modification of rhEGF and purification of PEG_x-rhEGF

The three primary amines on rhEGF allow PEG to be conjugated at up to three sites. The degree of PEG modification was controlled by pH since the N-terminus α-amine has a pKa of 7.8 while the ε-amines on Lys 28 and 48 have pKa's of 10.1[33]. Methoxy-PEG-propionaldehyde (mPEG-PPA) was used to synthesize PEG_1-rhEGF and PEG_2-rhEGF (Supplementary Fig. 2S). rhEGF was dissolved in 50 mM sodium acetate buffer (pH 5.0) to a final concentration of 1 mg/ml. 140 M excess $NaCNBH_3$ and either 3 (for PEG_1-rhEGF) or 6 (for PEG_2-rhEGF) molar excess of mPEG-PPA were added to the solution. The reaction was agitated for 1 h and incubated at room temperature for 23 h. The product solution was dialysed against 20 mM pH 5.0 sodium acetate buffer in 3.5 kDa MWCO slide-a-lyzer dialysis cassettes (Thermo Scientific, Rockford, IL, USA.). Greater than 80% yield of a pure population of PEG_1-rhEGF was obtained using 3 M excess of mPEG-PPA and a mixed population of PEG_1- and PEG_2-rhEGF (referred to as PEG_2-rhEGF) was produced using 6 M excess mPEG-PPA.

Methoxy-PEG-N-hydroxysuccinimide (mPEG-NHS) was used to synthesize PEG_3-rhEGF (Supplementary Fig. 2S). rhEGF was dissolved in 50 mM TES buffer (pH 8.6) to a final concentration of 0.33 mg/ml. Twenty-five molar excess of mPEG-NHS was added to the reaction mixture and the solution was agitated at room temperature for 2 h. Twenty-five molar excess of mPEG-NHS and 100 μl of TES buffer were added to the solution every 2 h until a total of 100 M excess of mPEG-NHS was reached. The NHS ester of PEG was selected for its higher reactivity compared to mPEG-PPA, and a pure population of pure PEG_3-rhEGF was produced using these reaction conditions (Supplementary Fig. 3S).

Upon completion, unreacted PEG was separated from the reaction mixture using fast protein liquid chromatography (UPC 900/P-920, Amersham Pharmacia Biotech, Piscataway, NJ, USA) with an anion exchange column (Pharmacia Biotech MonoQ, column volume ~7.7 ml). The ionic exchange gradient was set with a low-salt buffer (buffer A: 10 mM TES, pH 8.2) and a high-salt buffer (buffer B: 50 mM TES with 1 M NaCl, pH 8.2). Buffer A was first introduced into the column and a linear salt gradient up to 100% buffer B was established over 20 column volumes. The column was run with a flowrate of 2 ml/min. The purified product was analysed using gel electrophoresis (Bio-Rad Mini Format 1D electrophoresis system, Bio-Rad Laboratories, Mississauga, ON, Canada). The gel was stained for EGF using SimplyBlue SafeStain (Invitrogen, Burlington, ON, Canada) and then stained for PEG using a solution of 10% $BaCl_2$, 2.5% KI and 1.3% $I_{(s)}$ in distilled water. The gel images were taken on Bio-Rad Gel Doc XR 170-8170 and processed using Quantity One-4.6.1 software.

2.3. Fluorescent labelling of EGF and PEG-EGF

To allow real time imaging of protein transport, rhEGF and PEG_x-rhEGF were fluorescently labelled with Alexa 488. The Alexa dye was chosen for its relative pH stability and photostability [34]. For rhEGF, PEG_1-rhEGF and PEG_2-rhEGF, 1.6×10^{-4} M solutions of rhEGF or PEG_x-rhEGF were mixed with 10 M excess Alexa 488-NHS and the reaction was carried out for 2 h at room temperature. Unreacted dye was separated from fluorescent protein using a G25 Sephadex size exclusion column with 20 mM pH 7.4 PBS as running buffer. PEG_3-rhEGF was conjugated with Alexa 488-hydarzide using a 100 M excess DMTMM as

the coupling reagent. 25 M excess of the fluorescent dye was added to a 1.6×10^{-4} M PEG_3-rhEGF solution. The reaction mixture was agitated at room temperature for 24 h. Upon completion, excess Alexa 488 dye and DMTMM were separated from the product by dialysing the product solution against 50 mM TES buffer (pH 8.6) for 24 h.

The final protein concentration after fluorescent conjugation was determined by measuring the absorbance at 280 nm using NanoDrop ND-1000 spectrophotometer (NanoDrop, Wilmington, DE, USA) and correcting for the absorbance of the dye [35]. The protein and dye concentrations were determined by Beer's Law at an absorbance wavelength of 280 nm and an extinction coefficient of 17,780 M^{-1} cm^{-1} for rhEGF, and an absorbance at 495 nm and an extinction coefficient of 71,000 M^{-1} cm^{-1} for Alexa 488. The relative concentration of protein and fluorescent probe were used to determine the degree of fluorescent tagging. On average there is approximately one fluorescent molecule conjugated on each protein molecule (Supplementary Table 1).

2.4. Mouse surgeries

All experiments were carried out in accordance with the Guide to the Care and Use of Experimental Animals developed by the Canadian Council on Animal Care and approved by the Animal Care Committee at the University of Toronto. All animals used in this study were 8–10 week old C57BL/6 mice (Charles River, QC, Canada).

2.5. Mouse brain cortical slice preparations

Mice were sacrificed by cervical dislocation, the brain removed and immersed in 4 °C artificial cerebrospinal fluid (aCSF). The composition of aCSF is as follows: 124 mM NaCl; 5 mM KCl; 26 mM $NaHCO_3$; 1.25 mM NaH_2PO_4; 1.3 mM $MgCl_2$; 1.5 mM $CaCl_2$; and 10 mM D-(+)-glucose bubbled with 95% O_2/5% CO_2 (pH 7.0). Brains were mounted onto a specimen plate with the anterior of the brain pointed up with the dorsal surface of the brain perpendicular to the cutting blade and immersed in aCSF (4 °C). Coronal slices 400 μm thick were prepared from the interaural 4–5 mm plane using a microtome sectioning system (Series 1000, LR59590, Vibratome, Richmond, IL, USA) with a speed of 2.5 and amplitude of 9.0. Slices were transferred to aCSF (4 °C) and the temperature of the aCSF and brain slices were allowed to equilibrate to room temperature while bubbled with 95% O_2/5% CO_2. Individual slices were transferred to a Lab-Tek® II chambered #1.5 coverglass system and aCSF (37 °C) was added to the chamber immediately before imaging.

2.6. Cortical slice viability

The viability of cortical slices over time was determined using the lactate dehydrogenase (LDH) cytotoxicity detection kit (Roche Canada). Briefly, 400 μm cortical tissue slices were obtained and kept in oxygenated aCSF at room temperature. The slices were removed and placed into 48-well tissue culture plates at various times between 1 and 8 h post sacrifice. Slices were incubated for 1 h at room temperature in 500 μl aCSF without oxygenation to imitate the microinjection environment. One hundred microliters of the supernatant was then removed and the cytotoxicity assay was carried out according to the manufacturer's instructions. To determine the maximum concentration of LDH in cells, freshly prepared cortical slices were homogenized in 500 μl aCSF with 1.0 mm diameter Zirconia beads (BioSpec Products, 11079110zx, Bartlesville, OK, USA.) using a Mini BeadBeater tissue homogenizer (Biospec). The LDH assay was performed on the homogenate. All measurements were normalized to the homogenate LDH concentration. Measurements at all time points were performed on two slices from two individual animals.

2.7. Stroke surgeries

Stroke surgeries were carried out as described by Tennant et al. [36]. Mice were anesthetised with isoflurane, shaved and placed into a Kopf sterotaxic instrument. A midline insertion in the scalp was made. A small burr hole was made in the skull at the coordinates 2.25 lateral to the midline and 0.6 anterior to the Bregema. Using a 26 G needle, endothelin-1 (400 pM, Calbiochem, Gibbstown, NJ, USA.) was injected 1.0 ventral to the surface of the brain at a rate of 0.1 μl/min with a total volume of 1 μl. The needle was left in place for 10 min prior to removal to minimize back flow. The incision was sutured, antibiotic ointment applied and the animal left to recover under a heat lamp. Animals were sacrificed 4 days post-stroke and the cortical slices were prepared as described above for uninjured tissue.

2.8. Integrative optical imaging (IOI) to calculate protein diffusivity

Integrative optical imaging (IOI) was used to study the diffusion of proteins in *ex vivo* brain cortical slices as previously reported [13,22,23]. All protein samples were diluted with aCSF to a final protein concentration of 1.8×10^{-4} M prior to IOI. Intrinsic diffusivity (D) of rhEGF and PEG_x-rhEGF was determined through IOI in 0.3% agarose gel. The apparent diffusivities in brain were determined using 400 μm thick uninjured or stroke-injured mouse brain slices saturated with 0.1 mg/ml non-fluorescent rhEGF solution. This concentration was selected to ensure saturation of the cell-surface rhEGF receptors such that there is no elimination of fluorescently labelled proteins from the diffusion path. Finally to study the elimination of rhEGF and PEG_x-rhEGF in tissue, IOI was conducted in cortical tissue slices without pre-saturation.

A Nanoliter 2000 microinjection system (World Precision Instruments, Sarasota, FL, USA) was used to routinely inject 4.6 nl of fluorescently labelled protein solution into either agarose (Fig. 1b) or brain cortical slices at a depth of ~200 μm in the barrel field and trunk region of the primary somatosensory cortex, layers III–VI [37]. A minimum of 25 injections were made for each protein species in every diffusing medium. For diffusion in tissue, a minimum of 6 tissue slices prepared from 3 animals were used for each group. A fine-tip glass capillary with 1.2 mm outside diameter and 4 in. in length (World Precision Instruments, 1B120-4) was fire-polished to produce tips with 5 μm inside diameter (PUL 100 vertical pipette puller, World Precision Instrument) and used for injection. The evolution in the fluorescence over time was observed using a Zeiss Axio Observer Z1 epifluorescence microscope and captured with a Hamamatsu 13940RCA-ERA camera at 2 s interval. The intensity profiles of the diffusing source along a fixed axis were generated using the ImageJ (Image Processing and Analysis in JAVA, http://rsbweb.nih.gov/ij) analysis software, and quantitative analyses were conducted using Origin8 (OriginLab Corp.) and MATLAB (MathWorks).

2.9. Image analysis and mathematical modelling for estimating rate of elimination and protein penetration distance

Integrative optical imaging uses a point source-protein delivery, where the relationship between the diffusing protein concentration and the distance travelled at given time points is described by (Eq. (1)) [13]:

$$C_{free}(r,t) = \frac{UC_p\lambda^3}{\alpha[4D\pi(t+t_o)]^{3/2}} exp\left(\frac{-\lambda^2 r^2}{4D(t+t_o)}\right) exp[-k_e(t)] \quad (1)$$

where $C_{free}(r,t)$ is the free ECS protein concentration, U is the volume of protein solution injected, C_p is the concentration of injected protein solution, α is the volume fraction of ECM in the brain, typically assumed to be 0.2 [13]; r is the radial distance away from the injection

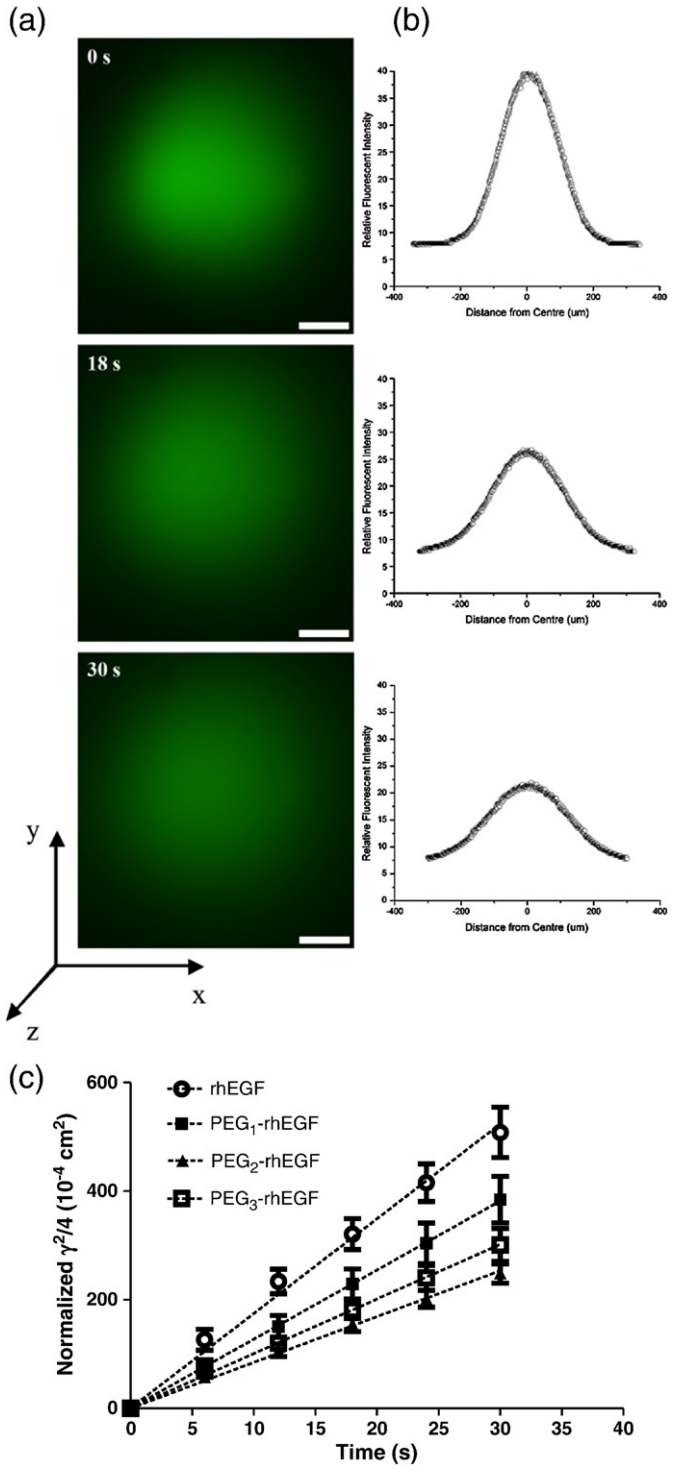

Fig. 1. Progression of rhEGF and PEG-rhEGF fluorescence intensity in dilute agarose following injection. (a) Representative images showing diffusion of fluorescently labelled rhEGF in dilute agarose. (b) Fluorescence intensity profiles obtained from images are fitted to Eqs. (2a) and (2b), where the vertical axis represents the fluorescent intensity in arbitrary units and the horizontal axis represents distance from the centre of the fluorescence. All images are shown at the same magnification (scale bar = 100 μm). (c) Representative graph showing plot of $\gamma^2/4$ (10^{-7} cm^2) vs. time (s) for (○) rhEGF, (■) PEG_1-rhEGF, (▲) PEG_2-rhEGF, and (□) PEG_3-rhEGF in agarose where values of $\gamma^2/4$ were obtained from fitting data to Eqs. (2a) and (2b), and the gradient of the plot returns a value of D (10^{-7} cm^2/s).

site, t is the time elapsed since injection, and t_o is the time required for a point source with a radius of zero to spread to the area that the protein occupies at the point of injection (t = 0).

In the absence of protein elimination from the diffusion pathway (*i.e.* $k_e = 0$), the intensity profile of the protein in the diffusing medium can be correlated to the effective diffusivity using the following set of equations (Eqs. (2a) and (2b)) [13]:

$$I_i(r,\gamma_i) = E_i\, exp\left[-\left({}^{r}/_{\gamma_i}\right)^2\right] \tag{2a}$$

$$\gamma_i = [4D\cdot(t+t_o)]^{1/2} \tag{2b}$$

where $I_i(r,\gamma_i)$ is the intensity at a radial distance away from the source measured by IOI and E_i is a de-focused point-spread function of the objective [13]. Numerical values of I_i were generated using ImageJ along an axis through the fluorescent image as a function of time and radial distance from the centre (Fig. 1), and the profile may be fitted in Origin 8 to generate the values of γ_i at specific time points (Fig. 1b). Graphing $\gamma_i^2/4$ (normalized such that the plot passes through the origin) vs. t yields a linear plot with gradient equal to the effective diffusivity D in the appropriate medium in the absence of elimination (Fig. 1c). A time frame of 30 s, over which the $\gamma_i^2/4$ vs. t plot remains linear, is typically used for determining the values of D. The tortuosity experienced by each protein species is determined from the diffusivities in the agarose and saturated cortical slices, as $\lambda = (D/D^*)^{1/2}$ [13].

When the protein is eliminated from the ECS during diffusion, the plot of $\gamma_i^2/4$ can be normalized to the diffusivity (D), and the $\gamma_i^2/4D$ vs. t yields a curve that deviate from linearity (Fig. 2b), indicating the effect of protein elimination. In this case we need to account for the contributions to total fluorescent intensity by both proteins in the ECS and the irreversibly-bound, non-mobile proteins. This may be estimated as (Eq. (3)):

$$I(r,t) = I_o C_{free}(r,t) + \varepsilon I_o C_{bound}(r,t) \tag{3}$$

where I_o is the proportionality constant between the local fluorescence intensity and protein concentration. Once the values of D and λ have been obtained using IOI in agarose and saturated tissue, we can estimate I_o by calculating the area under the fluorescent intensity peak at t_o. The approximate value of I_o determined here is approximately 0.1–0.5 nl/nmol AU, where AU is the arbitrary fluorescent intensity units. The parameter ε accounts for the decrease in detected intensity upon internalization. Since the time required for rhEGF/EGF receptor complex internalization varied between 5 and 30 min depending on the tissue type [38], which exceeds the time scale of IOI (3 min), we assumed the value of ε to be 1. From simple mass balance, the irreversibly-bound protein concentration $C_{bound}(r,t)$ may be described by (Eq. (4)):

$$C_{bound}(r,t) = k_e \int_0^t C_{free}(r,t)dt \tag{4}$$

Combining Eqs. (1), (3) and (4), an expression for the evolution in spatial fluorescence profiles is obtained (Eq. (5)):

$$I(r,t) = \frac{I_o C_p U \lambda^3}{\alpha[4\pi D(t+t_o)]^{3/2}} exp\left[-\frac{\lambda^2 r^2}{4D(t+t_o)}\right] exp[-k_e(t)] + \varepsilon I_o k_{bound} \int_0^t \frac{C_p U \lambda^3}{\alpha[4D(t+t_o)]^{3/2}} exp\left[-\frac{\lambda^2 r^2}{4D(t+t_o)}\right] exp[-k_e(t)]dt \tag{5}$$

We numerically solve this equation using MATLAB to obtain the values of *ke* since all other parameters may be either obtained from literature or determined experimentally. For each set of intensity profiles, the value of *ke* is iterated between 0 and 10^{-1} s^{-1} with an increment of 10^{-7} s^{-1}. The fitted value of *ke* yielding the least squares

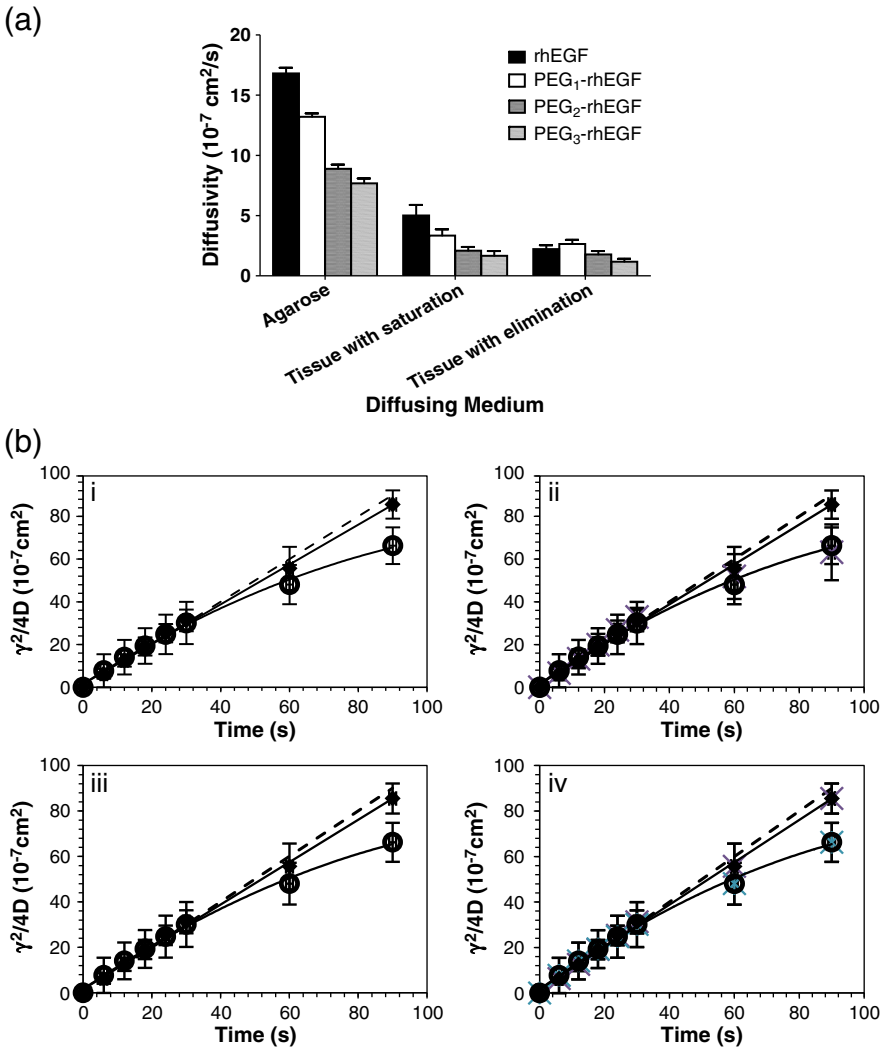

Fig. 2. PEG modification decreases diffusivity of rhEGF in saturated brain tissue. (a) Diffusivities for rhEGF and PEG$_x$-rhEGF are determined in agarose, saturated and non-saturated cortical tissue in uninjured animals. (b) Representative γ^2/4D vs. time plots of (i) rhEGF, (ii) PEG$_1$-rhEGF, (iii) PEG$_2$-rhEGF, and (iv) PEG$_3$-rhEGF diffusion in (■) saturated and (○) non-saturated tissue. Plot is linear in saturated tissue but deviates from linearity in non-saturated tissue.

residual (LSR) from the experimental data is taken to be the elimination constant.

We confirmed the method validity using agarose and saturated tissue. Since both agarose and saturated brain tissue should yield values of k_e equal to zero for any diffusing species, they serve as appropriate controls for the system. For rhEGF and PEG$_x$-rhEGF, the values of k_e calculated by the model were indeed 0 s^{-1}, confirming the validity of the model.

To ensure accuracy in fitting, the model-generated values of *ke* were used, along with experimental values of D and λ, to reproduce the series of theoretical intensity profiles with respect to time. These theoretical profiles were again fitted to Eqs. (2a) and 2b in Origin® to produce theoretical plots for γ^2/4D vs. time, which were compared with experimentally-derived plots of γ^2/4D vs. time (Supplementary Fig. 4S). Good agreement was found between all model fits and experimental data.

A polymer scaffold represents a constant source of protein drugs on top of the brain cortex, and the steady state concentration profile of the protein in the tissue can be represented as (Eq. (6)) [14,39]:

$$\frac{C}{C_o} = exp\left(\sqrt{\frac{k_e}{D}}\lambda x\right) \quad (6)$$

where C/C_o is the normalized concentration of protein at a certain distance, x, away from the source. Eq. (6) allows us to predict how far a protein can penetrate in the brain in the presence of a constant source before its concentration drops below the therapeutic threshold. Calculations are accurate to ±15%, as estimated by error propagation theory [40].

2.10. Total cell count in pre- and post-stroke brains

Four days following stroke, mice were transcardially perfused with 4% PFA, the brains were removed and cryoprotected overnight in 20% sucrose. Brains were sectioned coronally at 15 μm sections using a cryostat and placed on slides. Sections were viewed under a light microscope (Olympus CKX41). The lesion cavities were measured using ImageJ 1.38X to determine the epicentre of the lesion and pictures were taken of sections at the epicentre, 300 μm rostral and 300 μm caudal to the epicentre, using SonyIIDC version 1.2.0.2. Equivalent anatomical sections in control animals were stained with DAPI mounting media and coverslipped. The medial, ventral, and lateral areas surrounding the lesion cavity, contralateral cortex, or uninjured cortex were photographed using a fluorescent microscope (Zeiss Stemi 2000, KL1500 LCD) under 10× magnification. The total numbers of nuclei were counted per 276.25 mm² per region.

2.11. Real time RT-PCR to detect EGFR upregulation post-stroke

The upregulation of EGFR following stroke injuries was investigated using real time RT-PCR. Uninjured control animals and animals with 4 day stroke injuries were sacrificed, and the brains were harvested and divided along the midline to obtain the ipsilateral and contralateral hemispheres. Tissues were homogenized using Zirconia beads in a Mini BeadBeater tissue homogenizer. Extraction of mRNA was carried out as per the manufacturer's instructions (RNeasy Lipid Tissue Mini Kit, Qiagen) and OligodT primers were used to synthesize cDNA as per the manufacturers' instructions (AffinityScript Multi Temperature cDNA synthesis kit, Agilent Technologies). The following primers were used for cDNA amplification: 5′-GAA CTG GGC TTA GGG AAC TGC-3′ (EGFR forward); 5′-CAT TGG GAC AGC TTG GAT CAC-3′ (EGFR reverse) [41]. The house keeping gene used was hypoxantine phosphoribosyltransferase (HRPT): 5′-CTC ATG GAC TGA TTA TGG ACA GGA C-3′ (forward) and 5′-GCA GGT CAG CAA AGA ACT TAT AGC C-3′ (reverse), Real time RT-PCR was carried out using Lightcycler 480 II (Roche) with the following cycle: 95 °C, 60 °C, and 72 °C. A melt curve and gel electrophoresis were carried out to verify primer specificity.

2.12. In vivo penetration distance of rhEGF and PEG_1-rhEGF

The *in vivo* penetration distance of rhEGF and PEG_1-rhEGF in brain tissue was measured using uninjured animals. Mice were anesthetised with isofluorane and a small burr hole was made in the skull at the coordinates 2.25 lateral to the midline and 0.5 anterior to Bregema. A 30 gauge sterile Hamilton syringe was inserted 1.0 mm into the cortex and 0.5 μl of either protein or control solutions was injected. The injections were made at a rate of 0.1 μl/min, the needle was left in place for 10 min to reduce back flow, and the needle was retracted over 5 min. Treatment groups include sterile-filtered rhEGF or PEG_1-rhEGF solutions (8×10^{-5} M), saline controls, and mPEG-propionaldehyde dissolved in saline controls (8×10^{-5} M). Mice injected with protein solutions or control solutions were sacrificed at immediately (15 min), 4, and 24 h post injection.

Brains were extracted and snap frozen using $CO_{2(s)}$ cooled isopropane and stored at −80 °C. Three 1 mm coronal slices were prepared, at the injection site and rostral and caudal to the injection site. Coronal slices were prepared using McIlwain tissue chopper (790744-11, Mickle laboratory engineering company, Surrey, UK). Dorsal-ventral sections (0.5 mm) were then obtained from each coronal slice using Leica CM3050S cryostat system operating at −18 °C. Each 0.5 mm section was transferred into 2 ml polystyrene microtubes (Sarstedt 72.694.006, Montreal, Quebec, Canada) and 200 μl homogenizing buffer (20 mM HEPES, 10 mM KCl, 1.5 mM $MgCl_2$, 1 mM EDTA, 1 mM EGTA, 1 mM dithiothreitol, 1 mM PMSF) was added to each tube. Tissue sections were homogenized with 1.0 mm diameter zirconia beads. To remove tissue fragments, homogenized tissue was centrifuged at 15,000 RPM for 15 min at 4 °C and the homogenate was transferred into 1.75 ml Eppendorf tubes. 200 μl ELISA diluent solution was used to dilute homogenate to a total volume of 400 μl.

ELISAs were performed as per manufacturer's instructions on the homogenate solutions to determine the concentration of rhEGF at different depths from the cortical surface. Recombinant human EGF ELISA detection kit was used to avoid cross-contamination with endogenous mouse EGF. Protein concentrations detected in each animal were normalized to the amount of protein detected at the initial time to construct the diffusion profiles. A mass balance on the tissue rhEGF content showed that immediately post injection, approximately 90% of the injected protein was accounted for. The detectable concentration of proteins decreased over time, likely due to enzymatic degradation. Control groups injected with either saline solution or PEG dissolved in saline did not show detectable rhEGF concentrations at any of the time points studied (data not shown).

2.13. Bioactivity assay for neural stem cell response towards EGF and PEG_x-EGF

The bioactivity of rhEGF released from the DDS was determined *in vitro* using mice neural stem cell cultures. Neural stem cells were isolated from the subventricular zone (SVZ) of 9 week old male C57/BL6 mice and grown in 25 cm^2 tissue culture flasks (Corning CLS430639, Sigma Aldrich, Oakville, ON, Canada). Cells were passaged every 7 days for two weeks. Neurospheres were dissociated and plated in tissue culture treated 96-well plates (Corning CLS3696, Sigma Aldrich) at an initial cell density of 10 cells/μl in SFM and a total volume of 100 μl. rhEGF or PEG_x-rhEGF solutions were diluted in serum free culture media (SFM, 30% glucose, 7.5% $NaHCO_3$, 0.5% HEPES, 1% L-glutamine, 10% hormone mix, 1% Pen/Strep, 10% DMEM/F12, 74% dH_2O) and added to each well to a final concentration of 3.2 nM. The cells were incubated for 7 days at 37 °C without media change, following which MTT assays were performed as per manufacturer's instructions (Cell Titer 96, Promega) to evaluate metabolic activities of cells in culture.

2.14. Statistical analysis

The distribution of data was determined by the Kolmogorov–Smirnov normality test. For normally distributed data, comparisons between multiple groups were conducted using ANOVA. For pair-wise comparison of normally distributed data, t-test was carried out. For comparison of data that were not normally distributed, the Mann–Whitney-U test with Bonferonni correction was used [42]. Significance levels were indicated by $p<0.05$ (*), 0.01 (**), and 0.001 (***).

3. Results

3.1. The effect of PEG on the intrinsic diffusivity of rhEGF in agarose

Fluorescently labelled rhEGF and PEG_x-rhEGF (see Supplemental information: Fig. 1S, 2S and Table 1S) were separately injected into 0.3% agarose gels to study their intrinsic diffusivities. Dilute agarose gel was used to mimic a non-tortuous diffusing medium while avoiding convection. To calculate diffusivity, we injected fluorescently labelled proteins and monitored their intensity profiles over 30 s (Fig. 1a,b). By plotting the $\gamma^2/4$ parameter vs. time (Eqs. (2a) and (2b)) protein diffusivity was calculated from the slope, as shown in Fig. 1c. The intrinsic diffusivity (D) of rhEGF in agarose was 16.8×10^{-7} cm^2/s whereas that of PEG_x-rhEGF, where $x=1$, 2, or 3, was significantly less at 13.2×10^{-7} cm^2/s ($P<0.001$), 8.88×10^{-7} cm^2/s ($P<0.001$), and 7.68×10^{-7} cm^2/s ($P=0.0328$), respectively (Fig. 1c, Supplementary Table 2S). The decrease in intrinsic diffusivity of rhEGF with increasing PEG modification was likely due to its increase in hydrodynamic radius (R_H).

3.2. Transport of rhEGF and PEG_x-rhEGF in uninjured brain cortical slices

To understand the effect of tissue tortuosity on rhEGF vs. PEG_x-rhEGF diffusion independent of receptor binding, the EGF receptors (EGFR) of uninjured mouse brain cortical tissue slices were saturated with non-fluorescently-tagged rhEGF prior to the study. We also ensured that all brain tissue slices were >90% viable for over 8 h, which is longer than the duration of the diffusion study (Supplementary Fig. 5S).The apparent tissue diffusivity D^* of rhEGF (5.01×10^{-7} cm^2/s) decreased with PEG modification for PEG_1-rhEGF (3.34×10^{-7} cm^2/s), PEG_2-rhEGF (2.09×10^{-7} cm^2/s) and PEG_3-rhEGF (1.66×10^{-7} cm^2/s) (Fig. 2a; Supplementary Table 2S). There was a significant difference in D^* between all groups except for PEG_2-rhEGF and PEG_3-rhEGF

Table 1
Elimination rate constants in uninjured and stroke brains. Values of k_e were obtained by numerically solving Eq. (5) using the parameters listed in Supplementary Table S3. Values are reported as mean ± s.d. (n = 25).

Sample	Elimination rate (k_e (10^{-4} s^{-1}))		
	Ipsilateral to stroke injury	Contralateral to stroke injury	Uninjured brain cortical slices
rhEGF	659 ± 26.1[a b]	193 ± 21.2[a b]	52.0 ± 1.01[a b]
PEG_1-rhEGF	29.0 ± 2.99 [b]	19.7 ± 1.76 [b]	2.14 ± 0.24 [b]

[a] Values are significantly different from other values in the same column at $p<0.05$.
[b] Values are significantly different from other values in the same row at $p<0.05$.

($P=0.103$), likely due to an insignificant difference in R_H between PEG_2-rhEGF and PEG_3-rhEGF [18,43].

The tortuosity (λ) experienced by proteins in brain tissue was also calculated. In uninjured tissue, rhEGF experiences a λ of 1.83 whereas PEG_x-rhEGF had a λ of 1.99, 2.06, and 2.15 for $x=1$, 2, 3, respectively. Thus, the diffusion of smaller rhEGF is obstructed significantly less by the brain tissue than the larger, PEG-modified rhEGF ($p<0.001$).

The apparent diffusivity was calculated in tissue with elimination, where the tissue slices were not pre-saturated with non-fluorescent rhEGF. As in the case of pre-saturated tissue, the plot of $\gamma^2/4$ over 30 s revealed a significant decrease in D^* from rhEGF to PEG_3-rhEGF ($P=0.0054$, Fig. 2a, Supplementary Table 2S). The diffusivity of each protein species, however, was lower than in the former case. This decrease in apparent diffusivity likely reflects the binding of rhEGF to the ECM. Importantly, this decrease was dramatic for rhEGF (from 5.01 ± 0.88 for saturated to 2.22 ± 0.32 cm^2/s in non-saturated uninjured brain tissue) and insignificant for PEG-modified rhEGF (*e.g.*, from 3.34 ± 0.52 to 2.64 ± 0.35 cm^2/s), which suggests that PEG modification reduces the reversible binding of rhEGF to the ECM.

While the gradient of $\gamma^2/4D$ vs. time in saturated tissue remained linear, that in tissue with elimination deviated from linearity between 30 and 60 s, demonstrating the effect of protein elimination (Fig. 2b). In *ex vivo* tissue slices with elimination, although enzymatic degradation occurs over longer time scales [44], it is likely that rhEGF is primarily removed through either irreversible binding to the tissue, or cellular uptake. In an IOI experiment, this leads to the immobilization of the fluorescently-tagged growth factors, and thus a reduction in the slope of the $\gamma^2/4D$ vs. time curve.

Using the diffusivity and tortuosity determined above, we calculated the protein elimination rate constant k_e for rhEGF and PEG_x-rhEGF in uninjured tissue. This was achieved by fitting fluorescent intensity profiles in tissue with elimination over 3 min to Eq. (5) using MATLAB. Parameters used in the model are listed in Supplementary Table 3S. The k_e of rhEGF in uninjured tissue was determined to be 52.0×10^{-4} s^{-1} (Table 1) and those of PEG_x-rhEGF were 2.14×10^{-4} s^{-1}, 1.95×10^{-4} s^{-1}, and 1.45×10^{-4} s^{-1} for $x=1$, 2, 3 ($P<0.001$ for all 3 groups compared against rhEGF). The greatest difference in terms of reducing the rate of protein binding was between rhEGF and PEG_1-rhEGF, with a diminishing effect with di- and tri-PEG modification. This illustrates that PEG modification led to significantly slower protein elimination.

3.3. Transport of rhEGF and PEG_x-rhEGF in brain with stroke injury

To better understand the diffusion in brain tissue following stroke injury, the endothelin-1 (Et-1) stroke injury model was used [45,46] and tissue slices were taken after 4 days following the induction of stroke (Fig. 3a), thereby mimicking the time period previously studied for the delivery of rhEGF [10]. Given that proteins maintain bioactivity better after conjugation with one PEG compared to multiple PEG chains [47], and a significant reduction in the rate of protein elimination (k_e) for PEG_1-rhEGF was observed relative to rhEGF, the transport of rhEGF and PEG_1-rhEGF were compared in stroke-injured brain tissues (Fig. 3b, Supplementary Table 4S). As predicted from diffusivity data in agarose and uninjured tissue, D_{rhEGF}^* exceeded $D_{PEG1\text{-}rhEGF}^*$ in saturated tissue both ipsilateral ($P<0.001$) and contralateral ($P=0.007$) to the stroke injury. In saturated tissue, D_{rhEGF}^* ipsilateral to stroke was higher than both D_{rhEGF}^* contralateral to stroke ($P=0.0043$) and D_{rhEGF}^* in uninjured brain ($P=0.002$); yet no significant difference was observed for D_{rhEGF}^* between the contralateral hemisphere and the uninjured brain ($P=0.554$). These data indicate that stroke injury leads to change in tissue tortuosity.

To further investigate the effect of PEG modification on rates of rhEGF elimination in injured tissue, we calculated k_e both ipsilateral and contralateral to the stroke injury (Table 1). Consistent with observations in uninjured tissue, the k_e of PEG_1-rhEGF is 23-fold lower than rhEGF in tissue ipsilateral to stroke (29.0×10^{-4} s^{-1} vs. 659×10^{-4} s^{-1}, respectively) and 10-fold lower in tissue contralateral to stroke (19.7×10^{-4} s^{-1} vs. 193×10^{-4} s^{-1}, respectively). This demonstrates that PEG modification reduces the rate of protein removal from diffusion.

The difference observed for $D_{PEG1\text{-}rhEGF}^*$ in stroke vs. uninjured brains is likely due to a change in tissue composition following injury, discussed below. The tortuosity experienced by both rhEGF and PEG_1-rhEGF was lower in ipsilateral stroke injury tissue than both contralateral stroke injury tissue and uninjured brain tissue (Fig. 3c). Changes in tissue tortuosity could result from either changes in cell density or changes in the ECM. We determined that the total number of cells in stroke-injured brains and non-stroke brains were not significantly different between stroke ipsilateral, stroke contralateral and uninjured brain tissues (Fig. 3d,e).

We used real time RT-PCR to examine EGFR mRNA expression in the tissue. The results demonstrate that EGFR mRNA is significantly upregulated ipsilateral to the stroke injury compared to uninjured brain tissue ($P=0.014$; Fig. 3f), which could be accounted for by the increased expression in the ECM or cellular diversity within the injured tissue. EGFR expression contralateral to stroke does not differ significantly from uninjured controls ($P=0.166$). These data are consistent with the differences in tortuosity observed for rhEGF and PEG_1-rhEGF; however, they do not account for the differences observed for k_e ipsilateral and contralateral to stroke that are both significantly higher than that in uninjured brains (Table 1) for EGF and PEG_1-EGF. These data suggest that EGF/EGFR binding likely accounts for some, but not all, of the mechanisms influencing k_e.

3.4. Calculated penetration distance for rhEGF and PEG_x-rhEGF in brain cortical tissue

Based on the experimental D, λ and k_e values, we calculated the theoretical distance that rhEGF and PEG_1-rhEGF would diffuse in the cortex. Because this distance will depend on the duration of delivery, we analyze two limiting cases: (1) a pulse injection, as done in the case IOI; and (2) a constant source, as in the case of an ideal drug delivery scaffold. Because all drug delivery vehicles perform between these two limits, these calculations provide the "best- and worst-case" estimates on the theoretical diffusion distance. In each case, the penetration distance was estimated based on concentration of the free protein in the extracellular space, $C_{free}(r,t)$, using Eq. (1) for the pulse injection and Eq. (6) for the constant source (Fig. 4a). A meaningful estimation of penetration distance requires that the amount of protein reaching the target site maintains therapeutic benefit. Since NSCs proliferate *in vitro* at an rhEGF concentration of 3.2 nM (20 ng/ml) [48] and we found no difference in bioactivity between rhEGF and PEG_1-rhEGF at this concentration (Supplementary Fig. 6S), this value was used as $C_{free}(r,t)$ in Eqs. (1) and (6) to estimate rhEGF penetration distance.

In each case the penetration distance achieved from a constant source was greater than that achieved from a pulse injection (Table 2a and b). The penetration distance of PEG_1-rhEGF was also greater than that of rhEGF, regardless of the tissue type. In uninjured brain, we

(a)

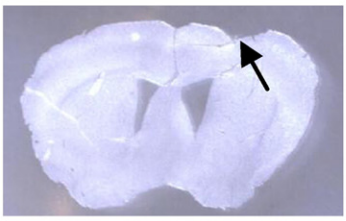

(b)

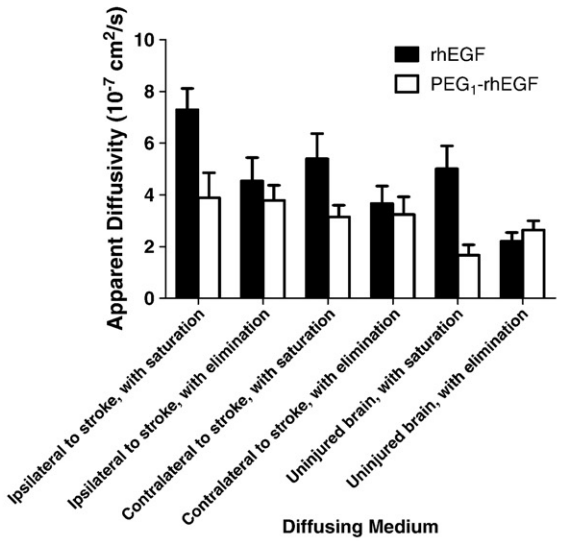

(c)

Sample	Calculated Tortuosity ($\lambda = (D/D^*)^{1/2}$)		
	Ipsilateral to Stroke	Contralateral to Stroke	Uninjured Tissue
rhEGF	1.52 ± 0.12 † **	1.76 ± 0.19 † **	1.83 ± 0.18 † **
PEG$_1$-rhEGF	1.84 ± 0.25 **	2.05 ± 0.16	1.99 ± 0.16 **

(d)

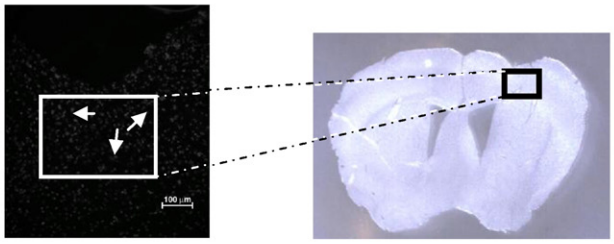

(e)

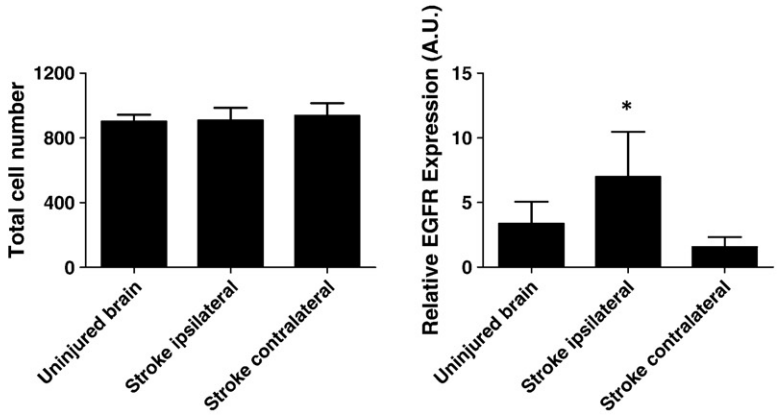

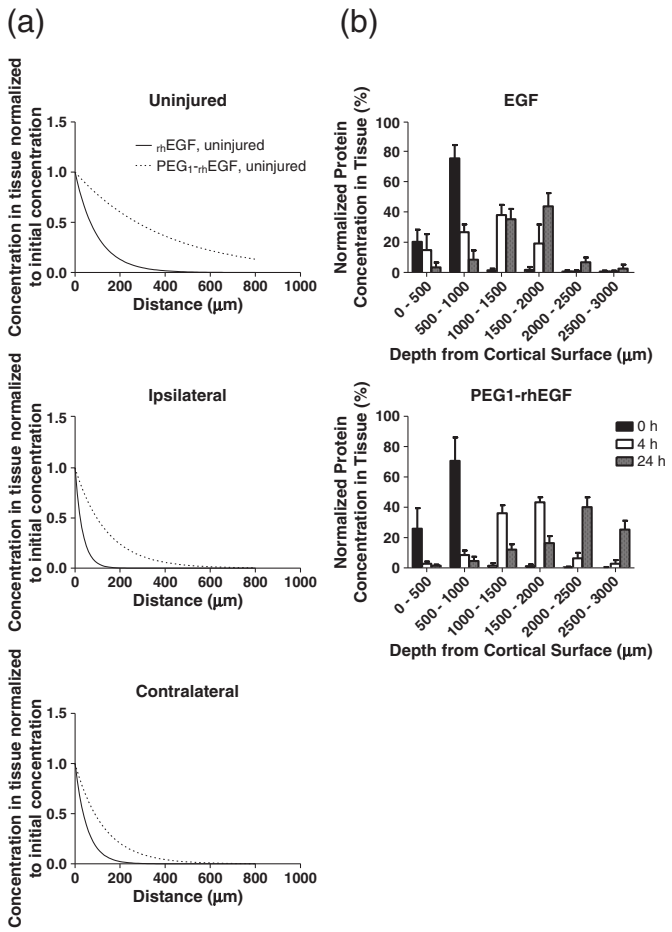

Fig. 4. PEG modification increases the predicted penetration distance of rhEGF, assuming constant source of protein. (a) Predicted penetration distances for PEG_1-rhEGF (dashed line) and rhEGF (solid line) in uninjured tissue, ipsilateral to stroke, and contralateral to stroke calculated using Eq. (6) (Methods). (b) PEG modification increases *in vivo* penetration distance of rhEGF following bolus injection. 0 h post injection, both rhEGF and PEG_1-rhEGF show maximum concentration at the site of injection (depth of 0.5–1 mm below the cortical surface). 4 h post injection, rhEGF shows peak concentration at 1.5 mm ventral to cortical surface while PEG_1-rhEGF concentration peaks at 2.0 mm. At 24 h post injection, rhEGF peak concentration occurs at similar depths as that at 4 h ($P = 0.594$), while PEG_1-EGF shows significantly further penetration compared to EGF. Values are reported as mean ± s.d. ($n = 4$).

calculate that rhEGF penetrates 1.5–1.8 mm while PEG_1-rhEGF penetrates to a distance to 4.4–7.0 mm. In injured tissue, rhEGF penetrated the tissue to 0.00–0.59 mm ipsilateral to stroke, likely due to rapid elimination, whereas PEG_1-rhEGF diffused 1.7–2.5 mm. Similarly, rhEGF penetrated 0.87–0.95 mm and PEG_1-rhEGF penetrated 1.8–2.3 mm in contralateral stroke-injured tissue. These results show that PEG modification increases the penetration distance of rhEGF, which falls within the range predicted by previous modelling studies [23].

3.5. In vivo penetration distance of rhEGF and PEG_1-rhEGF

To confirm our model predictions, we investigated the *in vivo* penetration distance of rhEGF and PEG_1-rhEGF in uninjured mouse brains. Bolus injections of protein solutions were made into the somatosensory cortex at the same coordinates used for Et-1 injections. The brains were then harvested and sectioned to analyze the rhEGF concentration at various depths by ELISA. We examined the diffusion profile of both native and PEG-modified rhEGF upon immediate sacrifice, and at 4 and 24 h after injection of the protein solutions (Fig. 4b). Immediately after injection we find the highest concentrations of both rhEGF and PEG_1-rhEGF at the site of injection (0.5–1 mm below the cortical surface). At 4 h after injection, rhEGF reaches a peak concentration at a depth of 1.0–1.5 mm from the cortical surface whereas PEG_1-rhEGF is found at a depth of 1.5–2.0 mm, demonstrating greater tissue penetration than native rhEGF. At 24 h after injection, the diffusion profile of rhEGF is similar to that at 4 h ($P = 0.594$) suggesting that a large fraction of the rhEGF is not freely diffusing between 4 and 24 h. In contrast, PEG_1-rhEGF penetrates significantly deeper by 24 h ($P = 0.003$ compared to 4 h) with the peak concentration found at 2.0–2.5 mm and significant concentration of PEG_1-rhEGF detected at 2.5–3.0 mm. The greater tissue penetration observed for PEG_1-rhEGF vs. rhEGF is consistent with our model predictions.

Table 2
Predicted penetration distance from a point source (a) and a constant source (b) by rhEGF and PEG_1-rhEGF in uninjured and stroke brains. Distances travelled are presented in units of millimetres. Diffusion is assumed to stop when concentration is less than 3 nM, which is the minimum EGF concentration required to stimulate NPCs *in vitro*.

(a)

Sample	Penetration distance from point source (mm)		
	Ipsilateral to stroke injury	Contralateral to stroke injury	Uninjured brain cortical slices
rhEGF	†	0.87	1.5
PEG_1-rhEGF	1.7	1.8	4.4

(b)

Sample	Penetration distance from constant source (mm)		
	Ipsilateral to stroke injury	Contralateral to stroke injury	Uninjured brain cortical slices
rhEGF	0.59	0.95	1.8
PEG_1-rhEGF	2.5	2.3	7.0

† Value is negligible.

4. Discussion

Stroke-injured brains differ from uninjured brains in cell and molecular composition as well as tissue organization [24,25,49,50]. For both rhEGF and PEG_1-rhEGF, we found D^* ipsilateral to stroke to be higher than that in uninjured brain. This suggests that the tissue surrounding the stroke site loses integrity following injury and the diffusing proteins encounter less tortuous resistance. Since the total cell counts in brain tissue pre- and post-stroke injury are similar, the difference in tortuosity may be due to changes in the brain ECM.

Both the intrinsic and apparent diffusivities of rhEGF in uninjured brain measured herein are consistent with values previously reported in the literature [13]. PEG modification of rhEGF leads to an increase in protein hydrodynamic radius, which results in decreased diffusivity [51]: the R_H of rhEGF increases approximately by a factor of 1.5 with the addition of one 5 kDa PEG chain, by an additional factor of 1.2 with the second 5 kDa PEG chain, and by smaller increments with subsequent PEG additions [43,52].

Fig. 3. PEG modification decreases diffusivity of rhEGF in saturated brain tissue. (a) Microscope image showing a mouse brain coronal section with the site of stroke injury indicated by black arrow, under 10× magnification. (b) PEG modification decreases diffusivity of rhEGF in brain with stroke. The effect of mono-PEG modification of rhEGF on tissue diffusivities is studied in ipsilateral and contralateral sides of stroke, as well as that in the absence and presence of elimination are also determined. (c) Calculated tortuosity of rhEGF and PEG_1-rhEGF in tissue. Tortuosities are reported as mean ± s.e.m. ($n = 25$). (d) Total cell number as determined by DAPI stain (scale bar = 100 μm). Arrows represent DAPI stained cells. (e) Total cell number is not elevated either ipsilateral or contralateral to stroke compared to uninjured controls. Cell counts are shown as mean ± s.e.m. ($n = 9$). (f) EGFR gene expression is upregulated post-stroke in the ipsilateral cortex. Real time RT-PCR results show that following stroke, the EGFR expression is upregulated ipsilateral to injury ($P = 0.014$).

While some reports have suggested that PEG modification is detrimental towards protein/receptor interactions, the specific influence of PEG modification is protein specific and concentration dependent [47]. Lee et al. showed that at concentrations above 1 nM, there was no significant difference in the binding affinity of EGFR to rhEGF and PEG_1-rhEGF [31]. We also found with an *in vitro* bioactivity assay that there is no difference in the metabolic response of NPCs to rhEGF orPEG_1-rhEGF at concentration of approximately 3 nM. Since rhEGF signalling relies on the binding between rhEGF and the extracellular domain of EGFR, this suggests that although PEG modification may retard the binding rate, the rhEGF/EGFR binding affinity is not significantly decreased. Moreover, the reduced rate of protein binding may be compensated through longer tissue residence time afforded by modification with PEG [47].

It is known that PEG masks protein surfaces against phagocytosis and enzymatic degradation, and may reduce protein interactions with cells and other ECM components in the diffusion path [43,53]. To the best of our knowledge, k_e for rhEGF in the brain has not been reported. Using a pure population of PEG-modified proteins and IOI, we quantitatively show for the first time that PEG modification leads to reduced rates of protein removal and increased protein penetration distances. In the context of IOI, protein elimination refers to the removal of protein from the diffusion pathway. Therefore k_e represents the rate of rhEGF/EGFR complex formation, non-specific rhEGF binding to the ECM, as well as endocytosis. Enzymatic degradation is not considered here because the time scale required exceeds that of IOI. The rhEGF/EGFR binding involves complex enzyme kinetics and the reported complex formation rates vary from $5\times10^{-2}\,s^{-1}$ to $3\times10^{-4}\,s^{-1}$ [54]. The rate of internalization following complex formation has also been investigated in a number of tissue types [55–59] and shown to vary between $5\times10^{-4}\,s^{-1}$ and $6\times10^{-3}\,s^{-1}$. Therefore our value of $k_{e,\ rhEGF}$ ($5.2\times10^{-3}\,s^{-1}$) in uninjured brain fall within these ranges and is a reasonable estimate.

Using IOI we found that binding of both rhEGF and PEG_1-rhEGF occurs most rapidly ipsilateral to stroke, with significantly slower elimination in uninjured tissue. This is likely because EGFR is upregulated after injury [38,60]. Interestingly, while the rate of elimination contralateral to stroke is lower than that ipsilateral to stroke, it is higher than elimination in uninjured brain tissue. This was unexpected since the contralateral side is often used as a control in studying disorders of the brain. Buga et al., however, found changes in gene expression profiles contralateral to stroke relative to uninjured tissues in aged animals [49]. This suggests that the contralateral hemisphere in stroke animals is also affected by stroke and not identical to uninjured brain tissue. Real time RT-PCR demonstrated that EGFR over-expression was observed ipsilateral, but not contralateral, to the injury. Thus while rhEGF/EGFR complex formation contributes to the change in k_e, it is not the sole determinant. Global changes in growth factor expression following stroke, for example, may facilitate other mechanisms that contribute to the increase in contralateral k_e, including changes in the ECM that lead to higher levels of non-specific protein adhesion to ECM components, as well as protein uptake by inflammatory cells.

The values of k_e reported here show that PEG modification can overcome the rapid elimination of protein drugs in diseased brains. Our results demonstrate the need to study protein transport in injured or diseased brain tissue (relative to control uninjured brains) because the rate of elimination impacts penetration distance and changes with tissue type. Rapid removal leads to shallow penetration distances and impacts the efficacy of drug delivery strategies.

The penetration distances calculated from IOI were confirmed *in vivo*. Between 4 and 24 h after a bolus injection of protein solutions, the PEG_1-rhEGF showed a 1.0 mm increase in penetration distance while the rhEGF itself demonstrated only a small change in tissue penetration distance. This suggests that more rhEGF was removed from the diffusing population compared to PEG_1-rhEGF. Our results are consistent with previous data showing increased penetration distance due to PEG modification. For example, Soderquist et al. illustrated that PEG modification of brain derived neurotrophic factor (BDNF) enhanced its *in vivo* half-life and tissue penetration [16]. Stroh et al. showed qualitatively that native BDNF undergoes negligible diffusion in the brain while a mixed population of PEG-BDNF, with various degrees of PEG modification, demonstrated significantly increased penetration [22]. Belcheva et al. demonstrated similar results where PEG-conjugated nerve growth factor improved its pharmacokinetic performance in the brain [21]. Similarly, Kang et al. found that conjugation of 5 kDa PEG to basic fibroblast growth factor (bFGF) increases its penetration distance in the spinal cord tissue [20]. In a related study, using dextran instead of PEG, Krewson et al. demonstrated that conjugation of a polymer to nerve growth factor increased tissue penetration [8]. Our finding demonstrates that PEG modification may enable the development of a less invasive strategy for delivering proteins to sites deep in the brain. PEG modification of growth factors provides a promising strategy for achieving minimally invasive and targeted protein therapy.

5. Conclusions

Current drug delivery strategies suffer from either an inability to obtain delivery profiles for optimum therapeutic efficacy or do not afford the level of minimal-invasiveness required in clinical applications. Quantification of the elimination constant demonstrated that PEG modification of rhEGF results in greater penetration in brain cortex. The calculated penetration distance was confirmed *in vivo* as PEG-modified rhEGF diffused deeper than the native form. While the actual penetration distance following release from a scaffold will be lower than that predicted by the constant source model due to protein depletion at the source, our findings suggest that the use of a controlled release, minimally invasive drug delivery system of PEG-rhEGF holds promise for strategies to repair the injured brain, including the stimulation of endogenous neural precursor cells.

Author contributions

Y.W — concept and design, collection and assembly of all data, data analysis and interpretation, developed the MATLAB program used for data analysis, manuscript writing, final approval of manuscript; M.J.C — concept and design, collection of all integrative optical imaging experiments, performed all surgeries and qPCR work, manuscript writing; R.G.W. synthesized and fluorescently labelled of PEG_3-rhEGF; Y.L. participated in initial stages of setting up the study and contributed to the mathematical model for data analysis. N.S. modified the stroke protocol originally developed by D.C., provided help with the surgeries, took images of brain slices and performed cell counts; C.M.M. — concept and design, data analysis and interpretation, manuscript writing; D. C. developed model of stroke, manuscript writing; M.S.S. concept and design, data analysis and interpretation, manuscript writing, final approval of manuscript.

Acknowledgements

We are grateful to Professor Phillip Choi and Yuri Shardt for assistance on MATLAB programming. We thank James Jonkman (AOMF) and Bruno Chue (Centre for Biological Timing and Cognition) for assistance with microscopy. We thank Jenny Chu for help with the cell counts and Marta Kovatcheva for help with the stroke model. We acknowledge funding from the Natural Science and Engineering Research Council (YW), the Ontario Neurotrauma Fund (MJC), the McMurrich Postdoctoral Fellowship (YL), Canadian Institute for Health Research (NS) and the Heart and Stroke Foundation (CMM, DC, MSS).

Appendix A. Supplementary data

Supplementary data to this article can be found online at doi:10.1016/j.jconrel.2010.10.022.

References

[1] Stroke and cerebrovascular accidents, World Health Organization, Circulation, 2009, <http://www.who.int/topics/cerebrovascular_accident/en/>.
[2] G.A. Ford, C.A. Bryant, A.A. Mangoni, S.H.D. Jackson, Stroke, dementia, and drug delivery, Br. J. Clin. Pharmacol. 57 (2004) 15–26.
[3] C. Wiltrout, B. Lang, Y.P. Yan, R.J. Dempsey, R. Vemuganti, Repairing brain after stroke: a review on post-ischemic neurogenesis, Neurochem. Int. 50 (2007) 1028–1041.
[4] C. Culmsee, J. Krieglstein, Ischaemic brain damage after stroke: new insights into efficient therapeutic strategies — International Symposium on Neurodegeneration and Neuroprotection, EMBO Rep. 8 (2007) 129–133.
[5] A.V. Kabanov, H.E. Gendelman, Nanomedicine in the diagnosis and therapy of neuro degenerative disorders, Prog. Polym. Sci. 32 (2007) 1054–1082.
[6] S. Weiss, B.A. Reynolds, A.L. Vescovi, C. Morshead, C.G. Craig, D. vanderKooy, Is there a neural stem cell in the mammalian forebrain? Trends Neurosci. 19 (1996) 387–393.
[7] T.D. Palmer, A.R. Willhoite, F.H. Gage, Vascular niche for adult hippocampal neurogenesis, J. Comp. Neurol. 425 (2000) 479–494.
[8] C.E. Krewson, W.M. Saltzman, Transport and elimination of recombinant human NGF during long-term delivery to the brain, Brain Res. 727 (1996) 169–181.
[9] J.M. Pean, M.C. Venier-Julienne, F. Boury, P. Menei, B. Denizot, J.P. Benoit, NGF release from poly(D, L-lactide-co-glycolide) microspheres, Effect of some formulation parameters on encapsulated NGF stability, J. Control. Release 56 (1998) 175–187.
[10] B. Kolb, C. Morshead, C. Gonzalez, M. Kim, C. Gregg, T. Shingo, S. Weiss, Growth factor-stimulated generation of new cortical tissue and functional recovery after stroke damage to the motor cortex of rats, J. Cereb. Blood Flow Metab. 27 (2007) 983–997.
[11] G. Grasso, A. Sfacteria, A. Cerami, M. Brines, Erythropoietin as a tissue-protective cytokine in brain injury: what do we know and where do we go? Neuroscientist 10 (2004) 93–98.
[12] A.G. de Boer, P.J. Gaillard, Strategies to improve drug delivery across the blood-brain barrier, Clin. Pharmacokinet. 46 (2007) 553–576.
[13] R.G. Thorne, S. Hrabetova, C. Nicholson, Diffusion of epidermal growth factor in rat brain extracellular space measured by integrative optical imaging, J. Neurophysiol. 92 (2004) 3471–3481.
[14] W.M. Saltzman, M.L. Radomsky, Drugs released from polymers — diffusion and elimination in brain-tissue, Chem. Eng. Sci. 46 (1991) 2429–2444.
[15] C.E. Krewson, R. Dause, M. Mak, W.M. Saltzman, Stabilization of nerve growth factor in controlled release polymers and in tissue, J. Biomater. Sci. Polym. Ed. 8 (1996) 103–117.
[16] R.G. Soderquist, E.D. Milligan, E.M. Sloane, J.A. Harrison, K.K. Douvas, J.M. Potter, T.S. Hughes, R.A. Chavez, K. Johnson, L.R. Watkins, M.J. Mahoney, PEGylation of brain-derived neurotrophic factor for preserved biological activity and enhanced spinal cord distribution, J. Biomed. Mater. Res. A 91A (2009) 719–729.
[17] P. Bailon, W. Berthold, Polyethylene glycol-conjugated pharmaceutical proteins, Pharm. Sci. Technol. Today 1 (1998) 352–356.
[18] C.J. Fee, J.A. Van Alstine, PEG-proteins: reaction engineering and separation issues, Chem. Eng. Sci. 61 (2006) 924–939.
[19] S.Y. Chen, S. Cressman, F. Mao, H. Shao, D.W. Low, H.S. Beilan, E.N. Cagle, M. Carnevali, V. Gueriguian, P.J. Keogh, H. Porter, S.M. Stratton, M.C. Wiedeke, L. Savatski, J.W. Adamson, C.E. Bozzini, A. Kung, S.B.H. Kent, J.A. Bradburne, G.G. Kochendoerfer, Synthetic erythropoietic proteins: tuning biological performance by site-specific polymer attachment, Chem. Biol. 12 (2005) 371–383.
[20] C.E. Kang, R. Clarkson, C.H. Tator, I.W.T. Yeung, M.S. Shoichet, Spinal cord blood flow and blood vessel permeability measured by dynamic computed tomography imaging in rats after localized delivery of fibroblast growth factor, J. Neurotrauma 27 (2010) 2041–2053.
[21] N. Belcheva, K. Woodrow-Mumford, M.J. Mahoney, W.M. Saltzman, Synthesis and biological activity of polyethylene glycol-mouse nerve growth factor conjugate, Bioconjug. Chem. 10 (1999) 932–937.
[22] M. Stroh, W.R. Zipfel, R.M. Williams, S.C. Ma, W.W. Webb, W.M. Saltzman, Multiphoton microscopy guides neurotrophin modification with poly(ethylene glycol) to enhance interstitial diffusion, Nat. Mater. 3 (2004) 489–494.
[23] M. Stroh, W.R. Zipfel, R.M. Williams, W.W. Webb, W.M. Saltzman, Diffusion of nerve growth factor in rat striatum as determined by multiphoton microscopy, Biophys. J. 85 (2003) 581–588.
[24] N. Futrell, Pathophysiology of acute ischemic stroke: new concepts in cerebral embolism, Cerebrovasc. Dis. 8 (1998) 2–5.
[25] S.C. Cramer, Repairing the human brain after stroke: I. Mechanisms of spontaneous recovery, Ann. Neurol. 63 (2008) 272–287.
[26] E. Spandou, S. Papoutsopoulou, V. Soubasi, G. Karkavelas, C. Simeonidou, G. Kremenopoulos, O. Guiba-Tziampiri, Hypoxia-ischemia affects erythropoietin and erythropoietin receptor expression pattern in the neonatal rat brain, Brain Res. 1021 (2004) 167–172.
[27] J. Scafidi, D.M. Fagel, L.R. Ment, F.M. Vaccarino, Modeling premature brain injury and recovery, Int. J. Dev. Neurosci. 27 (2009) 863–871.
[28] H.S. Lu, J.J. Chai, M. Li, B.R. Huang, C.H. He, R.C. Bi, Crystal structure of human epidermal growth factor and its dimerization, J. Biol. Chem. 276 (2001) 34913–34917.
[29] C.G. Craig, V. Tropepe, C.M. Morshead, B.A. Reynolds, S. Weiss, D. vanderKooy, In vivo growth factor expansion of endogenous subependymal neural precursor cell populations in the adult mouse brain, J. Neurosci. 16 (1996) 2649–2658.
[30] H.G. Kuhn, J. Winkler, G. Kempermann, L.J. Thal, F.H. Gage, Epidermal growth factor and fibroblast growth factor-2 have different effects on neural progenitors in the adult rat brain, J. Neurosci. 17 (1997) 5820–5829.
[31] H. Lee, T.G. Park, Preparation and characterization of mono-PEGylated epidermal growth factor: evaluation of in vitro biologic activity, Pharm. Res. 19 (2002) 845–851, (919).
[32] O.B. Kinstler, D.N. Brems, S.L. Lauren, A.G. Paige, J.B. Hamburger, M.J. Treuheit, Characterization and stability of N-terminally PEGylated rhG-CSF, Pharm. Res. 13 (1996) 996–1002, (922).
[33] J. McMurry, Fundamentals of Organic Chemistry, 5 ed., Thomson Brooks/Cole, 2003.
[34] N. Panchuk-Voloshina, R.P. Haugland, J. Bishop-Stewart, M.K. Bhalgat, P.J. Millard, F. Mao, W.Y. Leung, R.P. Haugland, Alexa dyes, a series of new fluorescent dyes that yield exceptionally bright, photostable conjugates, J. Histochem. Cytochem. 47 (1999) 1179–1188.
[35] M.P. Invitrogen, Amine-reactive Probes, 2009.
[36] K.A. Tennant, T.A. Jones, Sensorimotor behavioral effects of endothelin-1 induced small cortical infarcts in C57BL/6 mice, J. Neurosci. Meth. 181 (2009) 18–26.
[37] P.G., K.B.J. Franklin, The Mouse Brain in Stereotaxic Coordinates, 1 ed. Academic Press, 1996.
[38] B. Liu, H.Y. Chen, T.G. Johns, A.H. Neufeld, Epidermal growth factor receptor activation: an upstream signal for transition of quiescent astrocytes into reactive astrocytes after neural injury, J. Neurosci. 26 (2006) 7532–7540.
[39] C. Nicholson, Diffusion and related transport mechanisms in brain tissue, Rep. Prog. Phys. 64 (2001) 815–884.
[40] B.P. Levitt, An introduction to error analysis — the study of uncertainties in physical measurements — Taylor, Jr, J. Chem. Soc. Faraday Trans. I 79 (1983) 2269.
[41] L. Hammoud, D.E. Burger, X.R. Lu, Q.P. Feng, Tissue inhibitor of metalloproteinase-3 inhibits neonatal mouse cardiomyocyte proliferation via EGFR/JNK/SP-1 signaling, Am. J. Physiol. Cell Physiol. 296 (2009) C735–C745.
[42] H.H. Zar, Biostatistical Analysis, 3 edPrentice-Hall, Upper Saddle River, New Jersey, 1996.
[43] P. Caliceti, F.M. Veronese, Pharmacokinetic and biodistribution properties of poly (ethylene glycol)-protein conjugates, Adv. Drug Deliv. Rev. 55 (2003) 1261–1277.
[44] G. Carpenter, K.J. Lembach, M.M. Morrison, S. Cohen, Characterization of binding of I-125-labeled epidermal growth-factor to human fibroblasts, J. Biol. Chem. 250 (1975) 4297–4304.
[45] T.H. Murphy, D. Corbett, Plasticity during stroke recovery: from synapse to behaviour, Nat. Rev. Neurosci. 10 (2009) 861–872.
[46] V. Windle, A. Szymanska, S. Granter-Button, C. White, R. Buist, J. Peeling, D. Corbett, An analysis of four different methods of producing focal cerebral ischemia with endothelin-1 in the rat, Exp. Neurol. 201 (2006) 324–334.
[47] G. Pasut, F.M. Veronese, PEGylation of proteins as tailored chemistry for optimized bioconjugates, Polymer Therapeutics I: Polymers as Drugs, Conjugates Gene Deliv. Syst. 192 (2006) 95–134.
[48] V. Tropepe, M. Sibilia, B.G. Ciruna, T. Rossant, E.F. Wagner, D. van der Kooy, Distinct neural stem cells proliferate in response to EGF and FGF in the developing mouse telencephalon, Dev. Biol. 208 (1999) 166–188.
[49] A.M. Buga, M. Sascau, C. Pisoschi, J.G. Herndon, C. Kessler, A. Popa-Wagner, The genomic response of the ipsilateral and contralateral cortex to stroke in aged rats, J. Cell. Mol. Med. 12 (2008) 2731–2753.
[50] A.M. Comi, M.V. Johnston, M.A. Wilson, Strain variability, injury distribution, and seizure onset in a mouse model of stroke in the immature brain, Dev. Neurosci. 27 (2005) 127–133.
[51] F.M. Veronese, Peptide and protein PEGylation: a review of problems and solutions, Biomaterials 22 (2001) 405–417.
[52] C.J. Fee, Size comparison between proteins PEGylated with branched and linear Poly(Ethylene glycol) molecules, Biotechnol. Bioeng. 8 (2007) 725–731.
[53] S. Kubetzko, C.A. Sarkar, A. Pluckthun, Protein PEGylation decreases observed target association rates via a dual blocking mechanism, Mol. Pharmacol. 68 (2005) 1439–1454.
[54] E. Hellen, D. Axelrod, Kinetics of epidermal growth factor/receptor binding on cells measured by total internal reflection/fluorescence recovery after photobleaching, J. Fluoresc. 1 (2) (1991) 113–128.
[55] C.M. Waters, K.C. Oberg, G. Carpenter, K.A. Overholser, Rate constants for binding, dissociation, and internalization of Egf — effect of receptor occupancy and ligand concentration, Biochemistry 29 (1990) 3563–3569.
[56] H.S. Wiley, Anomalous binding of epidermal growth-factor to a431 cells is due to the effect of high receptor densities and a saturable endocytic system, J. Cell Biol. 107 (1988) 801–810.
[57] D.J. Knauer, H.S. Wiley, D.D. Cunningham, Relationship between epidermal growth-factor receptor occupancy and mitogenic response — quantitative-analysis using a steady-state model system, J. Biol. Chem. 259 (1984) 5623–5631.
[58] A.C. Myers, J.S. Kovach, S. Vukpavlovic, Binding, internalization, and intracellular processing of protein ligands — derivation of rate constants by computer modeling, J. Biol. Chem. 262 (1987) 6494–6499.
[59] C.E. Lloyd, M. Ascoli, On the mechanisms involved in the regulation of the cell-surface receptors for human chorio-gonadotropin and mouse epidermal growth-factor in cultured Leydig tumor-cells, J. Cell Biol. 96 (1983) 521–526.
[60] A.M. Planas, C. Justicia, M.A. Soriano, I. Ferrer, Epidermal growth factor receptor in proliferating reactive glia following transient focal ischemia in the rat brain, Glia 23 (1998) 120–129.